ARMY RESEARCH LABORATORY

Modeling the Penetration Behavior of Rigid Spheres Into Ballistic Gelatin

by Steven B. Segletes

ARL-TR-4393 **March 2008**

NOTICES

Disclaimers

The findings in this report are not to be construed as an official Department of the Army position unless so designated by other authorized documents.

Citation of manufacturer's or trade names does not constitute an official endorsement or approval of the use thereof.

Destroy this report when it is no longer needed. Do not return it to the originator.

Army Research Laboratory
Aberdeen Proving Ground, MD 21005-5069

ARL-TR-4393 **March 2008**

Modeling the Penetration Behavior of Rigid Spheres Into Ballistic Gelatin

Steven B. Segletes
Weapons and Materials Research Directorate, ARL

REPORT DOCUMENTATION PAGE	Form Approved OMB No. 0704-0188

1. REPORT DATE *(DD-MM-YYYY)*	2. REPORT TYPE	3. DATES COVERED (From - To)
March 2008	Final	September 2006–July 2007

4. TITLE AND SUBTITLE
Modeling the Penetration Behavior of Rigid Spheres Into Ballistic Gelatin

5a. CONTRACT NUMBER

5b. GRANT NUMBER

5c. PROGRAM ELEMENT NUMBER

6. AUTHOR(S)
Steven B. Segletes

5d. PROJECT NUMBER
AH80

5e. TASK NUMBER

5f. WORK UNIT NUMBER

7. PERFORMING ORGANIZATION NAME(S) AND ADDRESS(ES)
U.S. Army Research Laboratory
ATTN: AMSRD-ARL-WM-TC
Aberdeen Proving Ground, MD 21005-5069

8. PERFORMING ORGANIZATION REPORT NUMBER
ARL-TR-4393

9. SPONSORING/MONITORING AGENCY NAME(S) AND ADDRESS(ES)

10. SPONSOR/MONITOR'S ACRONYM(S)

11. SPONSOR/MONITOR'S REPORT NUMBER(S)

12. DISTRIBUTION/AVAILABILITY STATEMENT
Approved for public release; distribution is unlimited.

13. SUPPLEMENTARY NOTES

14. ABSTRACT
The penetration of 20% ballistic gelatin by rigid steel spheres is studied and analytically modeled. In order to properly capture the response for a wide variety of sphere sizes and impact velocities, a rate-dependent strength formulation is required for the ballistic resistance of gelatin.

15. SUBJECT TERMS
gelatin, penetration, rigid, sphere, rate-dependence

16. SECURITY CLASSIFICATION OF:			17. LIMITATION OF ABSTRACT	18. NUMBER OF PAGES	19a. NAME OF RESPONSIBLE PERSON
a. REPORT	b. ABSTRACT	c. THIS PAGE			Steven B. Segletes
UNCLASSIFIED	UNCLASSIFIED	UNCLASSIFIED	UL	36	19b. TELEPHONE NUMBER (*Include area code*) 410-278-6010

Standard Form 298 (Rev. 8/98)
Prescribed by ANSI Std. Z39.18

Contents

List of Figures

INTENTIONALLY LEFT BLANK.

1. Introduction

One may calculate the interface force, F, upon a projectile as the target's averaged flow stress applied over the directional component of the projectile's wetted area, to obtain

$$F/A_{p\_wet} = k_T \rho_T U^2 + R_T \quad , \tag{1}$$

where A_{p_wet} is the wetted area of the projectile, projected onto a plane perpendicular to the velocity vector, k_T is the target-flow "shape factor," ρ_T is the target density, U is the penetration velocity, and R_T is the so-called target resistance, an integrated amalgam of the deviatoric stress field developed in the target. For ductile eroding targets, many analyses have suggested (and experiments have supported) that the target resistance can be treated as a constant (*i.e.*, independent of penetration velocity) whose magnitude is in the range of four to six times the uniaxial flow stress of the material.

When the projectile erodes, the eroding nose of the projectile assumes a roughly hemispherical shape which is fully wetted by the erosion products. In this circumstance, one may reasonably assume that A_{p_wet} approaches the cross-sectional area of the projectile, A_P, and that k_T approaches the value of 0.5 associated with the Bernoulli stagnation pressure. The result is that the decelerative stress averaged over the cross section is given by

$$\bar{\sigma} = F/A_P = 1/2 \rho_T U^2 + R_T \quad . \tag{2}$$

Such a result is seen, for example, as part of the stress balance in the so-called extended-Bernoulli equation used by Tate (*1*) and others.

If, however, the projectile remains rigid during the penetration event, then a different set of simplifications apply. While it is deduced that the penetration velocity, U, must equal the projectile velocity, V, no simplifications are obvious regarding the shape factor and wetted area, k_T and A_{p_wet}, respectively. Thus, the cross-section-averaged decelerative stress is

$$\bar{\sigma} = F/A_P = (k_T \rho_T V^2 + R_T) \cdot A_{p\_wet}/A_P \quad . \tag{3}$$

When this equation is approximated by taking A_{p_wet} as A_P, with constant values of k_T and R_T, and when it is used as the decelerative stress acting upon the cross section of a rigid projectile, the form the equation takes is known as the Poncelet form.

The Poncelet form looks like

$$-M\dot{V} = BV^2 + C \tag{4}$$

and is traditionally solved by expressing the acceleration $\dot{V}$ as $V(dV/dx)$, where x is the coordinate of penetration. Given a striking velocity, V_0, the solution yields the penetration depth as a function of the current velocity:

$$x(V) = \frac{M}{2B} \log\left(\frac{C + BV_0^2}{C + BV^2}\right) \quad . \tag{5}$$

The final penetration depth is obtained when the instantaneous velocity, V drops to zero, to yield

$$P(V_0) = \frac{M}{2B} \log\left(1 + \frac{B}{C}V_0^2\right) \quad . \tag{6}$$

Segletes and Walters (2) also offered a time-dependent explicit solution to the Poncelet form (*i.e.*, in terms of $V(t)$ and $x(t)$, where t is the time variable) when they solved for the residual rigid-body penetration phase of an otherwise eroding-body event. The form of their solution, using the nomenclature of equation 4, is

$$V(t) = \sqrt{\frac{C}{B}} \tan\left[\frac{\sqrt{BC}}{M}(t_f - t)\right] \tag{7}$$

and

$$x(t) = \frac{M}{B}\left\{\log\cos\left[\frac{\sqrt{BC}}{M}(t_f - t)\right] - \log\cos\left(\frac{\sqrt{BC}}{M}t_f\right)\right\} \quad , \tag{8}$$

where the event duration, t_f, is given by

$$t_f = \frac{M}{\sqrt{BC}} \tan^{-1}\left(V_0\sqrt{\frac{B}{C}}\right) \quad . \tag{9}$$

It can be shown, through trigonometric substitution, that x for the case of $V = 0$ in equation 5 is identical to x for the case of $t = t_f$ in equation 8. This is as it should be since the total penetration should not depend on whether V was integrated over t or x.

2. Theory

Presently, we wish to model the penetration of gelatin by rigid spheres. To do so, we will re-examine the data of Sturdivan (*3*) and Minisi (*4*). Sturdivan modeled the gelatin by considering the effects of inertial and viscous deceleration using a generalization of Resal's law. Gelatin strength was not part of Sturdivan's model. As a result, the latter stages of penetration tended to be overestimated since viscous deceleration loses its potency at diminished velocity *vis*-à-*vis* strength-based deceleration. In the current approach, a rate-based strength is introduced, allowing one to bridge the gap between pure viscous and pure strength-based velocity retardation models.

In hopes of simplifying equation 3 to a useful, solvable form that is nonetheless more general than the Poncelet form, we will make several assumptions *a priori* and later determine their appropriateness. First, we will assume k_T and A_{p_wet}/A_P to be constant. We will generalize the target resistance R_T (*i.e.*, the flow stress) to be a material property that is not constant as in the Poncelet form but instead dependent upon a power of the characteristic strain rate, $\dot{\epsilon}$.

Therefore, from equation 3, we have

$$F/A_P = 1/2\rho_T \cdot [bV^2 + V_c^2(\dot{\epsilon}/\dot{\epsilon}_c)^\alpha] \quad , \tag{10}$$

where b, α, V_c, and $\dot{\epsilon}_c$ are constants (b and α are dimensionless) that have been introduced in a manner compatible with our assumptions. A characteristic strain rate may be conveniently defined as

$$\dot{\epsilon} = 2V/D \quad , \tag{11}$$

where D is the projectile diameter ($D/2$ is the characteristic length of shearing strain). With the form of equation 10 and in light of equation 11, the instantaneous drag coefficient may be expressed as

$$C_D = \frac{F}{1/2\rho_T V^2 A_P} = b + \left(\frac{D_c}{D}\right)^\alpha \left(\frac{V_c}{V}\right)^{2-\alpha} \quad . \tag{12}$$

Note that since the penetrator remains rigid, the sphere diameter of equation 12 is a constant parameter for any given test, varying only when the projectile is changed for

different test cases. However, the dependence of C_D on instantaneous velocity V means that for a target material with strength, the drag coefficient will change (*i.e.*, increase for typical α) during the course of deceleration.

For an eroding configuration into a traditional Tate-like ductile target material, the value of b would equal unity and the exponent α would be zero. In contrast, for a rigid penetrator in a constant-drag fluid (*e.g.*, for a laminar Newtonain fluid at moderate Reynolds number, $2000 < R < 250,000$), the value of b would equal the fixed drag coefficent (approximately 0.4 for a sphere in Newtonian fluid, see figure 1) and the values of V_c would equal zero.

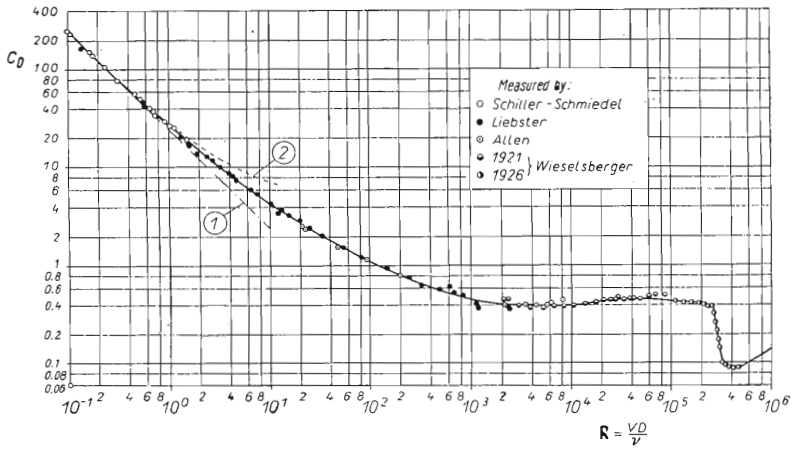

Figure 1. Drag coefficients for spheres traversing Newtonian fluid as a function of Reynolds number (*5*).

For the special case of $\alpha = 1$ in which the flow stress of the target is directly proportional to the strain rate (*i.e.*, when the material behaves as a Newtonian fluid), the drag form of equation 12 for vanishing V will mimic the low-Reynolds-number Stoke's formula for drag upon a sphere. Thus, we see that the form we have chosen in equation 10, merely through the selection of parameters α and b, can be made to emulate material behavior somewhere between an ideal ductile solid ($\alpha = 0$ and $b = 1$) and a laminar Newtonian fluid (very approximately, $\alpha = 1$ and $b = C_{D(\text{steady})}$).

When the retardation force is formulated according to equation 10, the resulting equation of motion becomes

$$-(M/A_P) \cdot \dot{V} = 1/2\ \rho_T \cdot [bV^2 + V_c^2(\dot{\epsilon}/\dot{\epsilon}_c)^\alpha] \quad . \tag{13}$$

Substituting for the geometric terms as well as the strain rate, $\dot{\epsilon}$, allows one to obtain the formulation in terms of V and D:

$$-\left(\frac{\rho_P}{\rho_T}\right) 2L_{eff}\dot{V} = bV^2 + \left(\frac{D_c}{D}\right)^{\alpha} V_c^{2-\alpha} V^{\alpha} \quad , \tag{14}$$

where the effective length, L_{eff}, can be characterized as the projectile volume divided by the projectile's presented area when projected onto a plane perpendicular to the velocity vector. For the present case of a spherical projectile, the term $2L_{eff}$ simply becomes $(4/3)D$.

Having formulated a flow-retardation form for rigid spheres (equation 14) that is more general than the Poncelet form (equation 4) we must now derive the solution to it. Using the standard approach of decomposing $\dot{V}$ as $V\,dV/dx$, equation 14 can be reformulated into:

$$\frac{-V^{1-\alpha}dV}{bV^{2-\alpha} + (D_c/D)^{\alpha} V_c^{2-\alpha}} = \frac{3}{4}\left(\frac{\rho_T}{\rho_P}\right)\frac{dx}{D} \quad . \tag{15}$$

Such a form is directly integrable over the velocity limits V_0 to V as

$$\frac{3}{4}\left(\frac{\rho_T}{\rho_P}\right)\frac{x}{D} = \frac{1}{b(2-\alpha)} \log\left[\frac{1 + b\,(D/D_c)^{\alpha}\,(V_0/V_c)^{2-\alpha}}{1 + b\,(D/D_c)^{\alpha}\,(V/V_c)^{2-\alpha}}\right] \quad . \tag{16}$$

For the case where penetration ceases at $V = 0$, one obtains the total penetration, P, as

$$\frac{3}{4}\left(\frac{\rho_T}{\rho_P}\right)\frac{P}{D} = \frac{1}{b(2-\alpha)} \log\left[1 + b\,(D/D_c)^{\alpha}\,(V_0/V_c)^{2-\alpha}\right] \quad . \tag{17}$$

Unfortunately, no time-based solution, comparable to that given in equations 7–9 has been obtained for this more general case. However, for certain select values of α, additional progress may be had, as will be subsequently explored. Regardless, equation 17 provides a solution which can be compared against aggregated penetration *vs.* striking-velocity data, while equation 16 can be used to examine the deceleration characteristics of individual tests, for which P vs. V data have been extracted. With a target-material description that is a function of strain rate, however, normalized penetration, P/D, is no longer independent of projectile diameter.

Fitting equation 17 would appear to require the specification of four fitting parameters, b, α, D_c, and V_c. However, the terms involving the parameters V_c and D_c can, in fact, be grouped together as $V_c^{2-\alpha}D_c^{\alpha}$ and therefore represent a single independent parameter. In

practice, D_c is arbitrarily taken as the sphere diameter for which some test data is available, and V_c is fit accordingly.

For certain select values of α, additional progress may be had in obtaining analytical solutions. The fortuitous fitting of the α parameter to a value of $1/2$ will provide such an opportunity. In this case, one may begin with equation 14, using the substitution of $z^2 = V$, in order to arrive at the form

$$-\frac{3\rho_T dt}{8\rho_P D} = \frac{dz}{bz^3 + a} \quad , \tag{18}$$

where

$$a = \left(\frac{D_c}{D}\right)^{1/2} V_c^{3/2} \quad . \tag{19}$$

While a contains the diameter D, which can vary from test to test, the integration required of equation 18 is not adversely affected since a remains constant for any given test case. This form is directly integrable (*6*) and yields, upon resubstitution for V,

$$\frac{3\rho_T}{8\rho_P D} t = \frac{k}{3a}\left[\frac{1}{2}\log\frac{(k+\sqrt{V})^3}{a+bV^{3/2}} + \sqrt{3}\tan^{-1}\frac{2\sqrt{V}-k}{k\sqrt{3}}\right]_V^{V_0} \quad , \tag{20}$$

where

$$k = \sqrt[3]{\frac{a}{b}} \quad . \tag{21}$$

Once $t(V)$ is known through equation 20 and given that $x(V)$ is known through equation 16, one can construct x *vs.* t as an implicit function of V for this very special case of $\alpha = 1/2$.

3. Results

The presentation of data *vis-à-vis* the model is complicated by the fact that the available data cover a range of sphere diameters and not all of the collected data span the complete test. For example, the tests of Sturdivan (*3*) terminated data collection while there was still significant residual velocity in the penetrator.

It should also be noted that the reporting of penetration into gelatin is further complicated by the presence of a large elastic recoil in the target. Because of this recoil,

the *final* penetration can be somewhat less than the point of *maximum* penetration, which occurs prior to the recoil. Arguments can be made for the use of either metric as the more appropriate measure of penetration. However, because the current model (which ignores recoil) is intended to be used to predict the time-response of penetration, this report uses the *maximum* penetration to define *the* penetration.

It is perhaps easiest, therefore, to navigate through the results by first presenting the fitted parameters, then examining the functional behavior of the model with those parameters, and finally, showing how the sundry experimental data compare with the model.

3.1 Model Parameters and Qualitative Behavior

The parameter D_c was arbitrarily selected as 4.445 mm (0.175 in), corresponding to the sphere diameter employed in a number of tests by Minisi (*4*) into 20% ballistic gelatin. The other model parameters were fitted to equation 17 using the data of Sturdivan (*3*) and Minisi (*4*). In the case of Minisi, $x(t)$ data were provided directly in tabular form, while in the case of Sturdivan, the $x(t)$ data were digitized from plots. In both cases, central differencing was employed to estimate the instantaneous slope of the $x(t)$ curve (representing $V(t)$).

With this technique, and using the more extensive data set of Sturdivan spanning three sphere diameters and striking velocities out to 2229 m/s, the remaining model parameters were fitted. Their values are given in table 1. In the case of Minisi's more limited data set, all fitted parameters remained the same except V_c, which was best fit as 105 m/s. We will take the fits to the Sturdivan dataset as the baseline set of fitted parameters to examine here. Note, however, that in both cases, the fitted value of α is $1/2$, which fortuitously allows for the employment of equation 20 if the time response of

Table 1. Model parameter fits.

Parameter	**Sturdivan Data (baseline)**	**Minisi Data**
α	0.5	0.5
b	0.34	0.34
D_c(mm)	4.445	4.445
V_c(m/s)	85	105

the deceleration is desired.

First, we examine how this model predicts normalized penetration *vs.* striking velocity for spheres of different diameters. Figure 2 shows how the sphere diameter affects the normalized penetration profiles. All these curves would collapse into a single curve if the strain rate dependence were absent (*i.e.*, if $\alpha = 0$). As it is, however, the strain-rate dependence significantly lowers the normalized penetration as the sphere diameter is decreased. The figure includes curves for a number of sphere diameters, including the three (ranging from 2.38 mm to 6.35 mm) tested by Sturdivan (*3*) that were also used to fit the model parameters (to be later examined in greater detail).

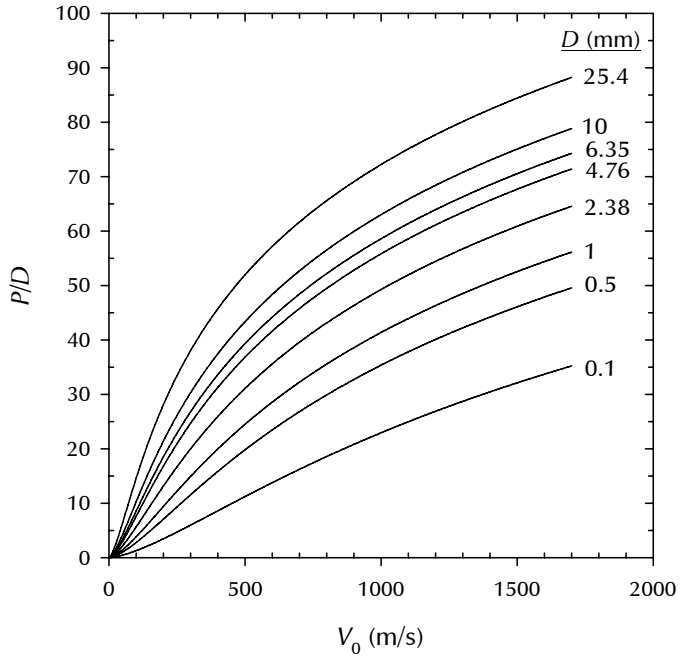

Figure 2. Normalized penetration of steel sphere into 20% ballistic gelatin, predicted as a function of striking velocity, with sphere diameter as a parameter.

Figure 3 considers the situation for one diameter of sphere (10 mm) and examines the penetration that is achieved as the sphere is decelerated to a particular fraction of the striking velocity (V_r/V_0). Here, the term V_r refers to the residual velocity possessed by the penetrator upon penetrating a certain depth of gelatin. Because the penetrator is rigid, however, V_r also represents the instantaneous penetration velocity. While the numerical values of residual and penetration velocity will be equal, the distinction is whether attention is being called to the behavior of the penetrator or the target,

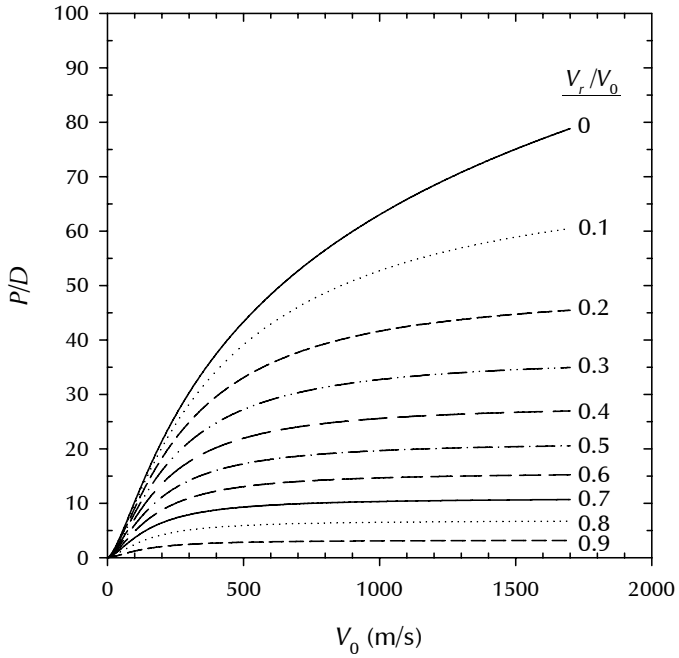

Figure 3. Normalized penetration for steel sphere (D = 10 mm) into 20% ballistic gelatin, predicted as a function of striking velocity, with relative residual velocity, V_r/V_0, as a parameter.

respectively. The larger spacing between the low-residual-velocity curves (at high striking velocity) indicates that the greatest penetration efficiency occurs at these lower penetration velocities. Such a result is not wholly unexpected since the strain-rate dependence of the model is one that yields a stronger target at higher strain rates (*i.e.*, at higher instantaneous penetration velocities).

The horizontal flatness of the curves at higher striking velocity indicates that for a fixed percent residual-velocity degradation, a fixed penetration is obtained, regardless of the actual striking velocity. This result represents the solution to any inertially driven problem (*i.e.*, where strength is a small fraction of the inertial force) and is not a function of the strain-rate dependence of the target material.

Rather than portraying the information in terms of relative residual velocity, as in figure 3, the same information can be displayed in terms of the abolute residual velocity. This is done in figure 4, which reveals a few additional subtleties compared to figure 3. While the same basic trend of higher penetration efficiency at lower penetration

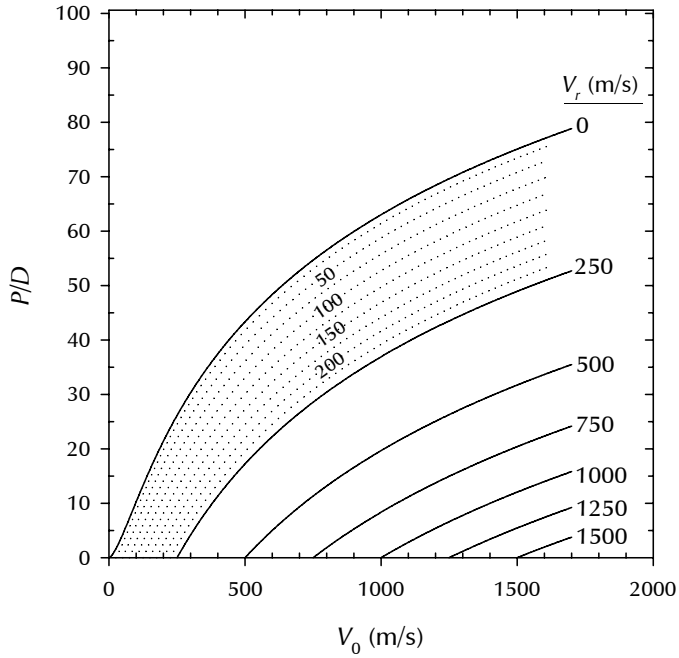

Figure 4. Normalized penetration for steel sphere (D = 10 mm) into 20% ballistic gelatin, predicted as a function of striking velocity, with residual velocity, V_r, as a parameter.

velocities is quite apparent (*e.g.*, for V_r below 250 m/s), figure 4 shows that this trend has its limits at low striking velocities. For V_r below 25 m/s, the efficiency drops precipitously. This reversal is due to the fact that at *very* low penetration velocities, the inertial term is becoming dwarfed by the strength magnitude, even as the strength term is itself decreasing. For the data fit being considered, optimal penetration efficiency appears to occur in the range of 50–150 m/s, though it remains relatively high to penetration velocities approaching 500 m/s.

Another interesting representation of the model can be considered by comparing the drag coefficient as a function of the Reynolds number for the current gelatin model *vs.* the data that exists for spheres traversing purely Newtonian fluids. This comparison is displayed in figure 5, specifically for spheres of 2.38 mm and 6.35 mm diameter *vis*-à-*vis* Newtonian flow. To estimate the Reynolds number in gelatin, a value for viscosity had to be established. And while viscous drag is not part of the current gelatin model, a value was selected based on estimates of Sturdivan (3). Taking Sturdivan's boundary-layer thickness as the radius of the sphere, the value of μ/D takes on a

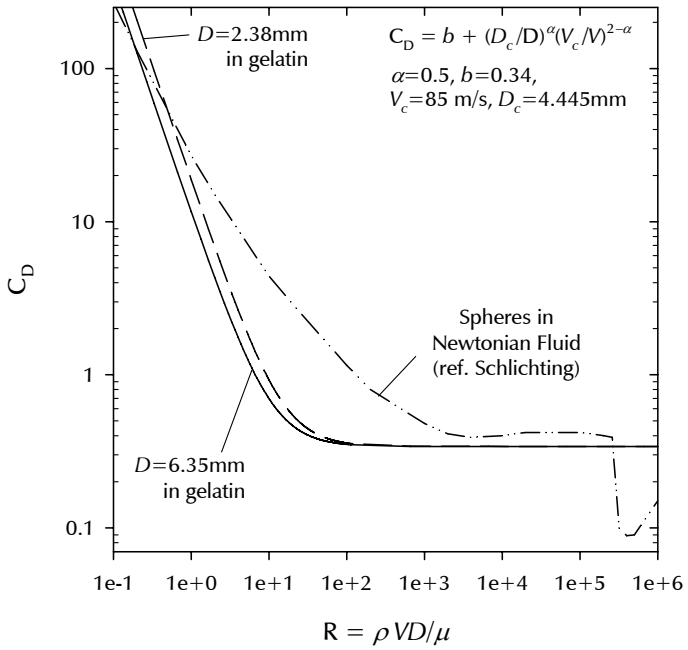

Note: The curve for spheres in Newtonian fluid was adapted from (*5*) in figure 1.

Figure 5. Drag coefficient *vs.* Reynolds number for 2.38 mm and 6.35 mm spheres penetrating gelatin *vis*-à-*vis* a Newtonian fluid .

constant value of 15,000 Pa·s/m. To repeat, this value was used merely to establish a Reynolds number in gelatin for comparative purposes and is not an integral part of the current strength-based gelatin model. The effect on the figure of selecting a different value for μ/D would be to shift the model curves horizontally (to the left if μ/D were increased and to the right if it decreased). Such a variation will not invalidate the inferences to be drawn about the qualitative behavior of the drag coefficient in gelatin.

The comparison shown in figure 5 reveals several salient points. First, with decreasing Reynolds numbers, the gelatin drag rises more steeply than the Newtonian data. This feature occurs because shear strength is a component of the gelatin drag, whereas it is not in Newtonian fluids. As the penetration velocity (*i.e.*, the Reynolds number) is decreased, the influence of the strength term becomes more prominent.

The other important point to draw is that in the flat (*i.e.*, steady-state) range of laminar flow, drag in gelatin is somewhat less than that in Newtonian fluids (a drag coefficient of 0.34 as compared with approximately 0.40). This behavior of gelatin is believed to arise

from the gelatin's tensile strength. In particular, the strength of gelatin serves to retard the tension-induced flow separation by providing an ability to withstand some level of tension as the flow approaches the waist of the sphere. The retarded separation produces what can only be described as a more streamlined flow *vis*-à-*vis* a Newtonian fluid, having the net effect of lowering the form drag upon the sphere.

The sharp adjustment of Newtonian drag for $R > 10^5$ depicts the effect of a transition from laminar to turbulent flow. To this point, no evidence of such a transition in gelatin has been observed, though it is not exactly clear what form turbulance might take in a viscoelastic solid.

3.2 Comparison to Experimental Data

Having laid out the form and functional behavior of this strain-rate dependent gelatin model, one may turn to a comparison with ballistic data of sphere penetration into 20% gelatin. Surdivan (*3*) presented data in the form of penetration *vs.* time. Data collection often ceased while there was still forward motion of the sphere. To represent his data for this report, Sturdivan's graphs were digitized in order to estimate late-time penetrations and associated residual velocities. More recently, Minisi (*4*) has collected low-velocity impact data for steel spheres into gelatin. Minisi's data has the virtue of being collected out to the point where forward velocity of the sphere ceased.

Because the predicted response is dependent upon the projectile diameter, it will prove easist to present comparisons for each respective sphere size for which data is available. In all cases, however, it is the same model parameters described in the prior section of this report which are used for the model predictions of the data, for all projectile diameters. Namely, these parameters take on the values depicted in table 1.

First, we consider 2.38 mm-diameter steel-sphere data collected by Sturdivan, corresponding to a mass of 0.85 gr. The results are shown in figure 6. Predictions for the low-velocity impacts are quite insensitive to small amounts of residual velocity because the sphere deceleration is quite pronounced at these low velocities. The high velocity data above 2000 m/s are likewise matched very well by the model.

Next, we consider Sturdivan's data for 7 gr. steel spheres with 4.76 mm diameters. The comparison to the model is shown in figure 7. Both experimental data are matched closely by the model.

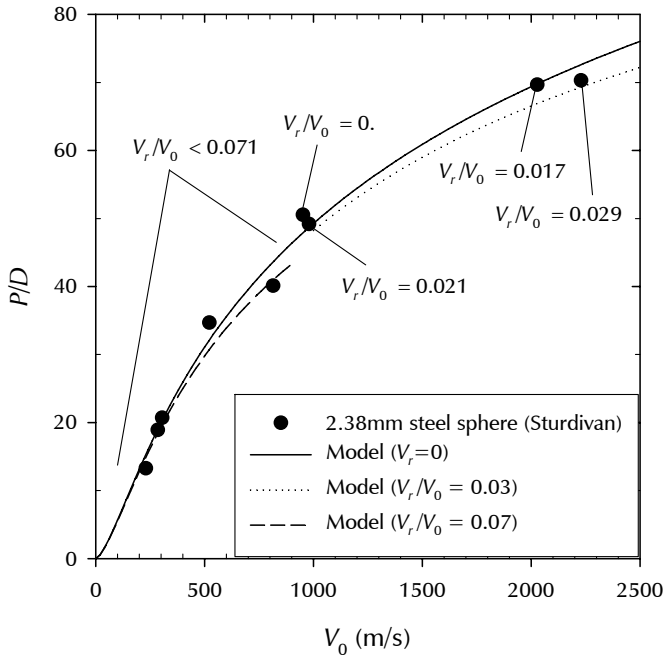

Figure 6. Normalized penetration *vs.* striking velocity for 2.38 mm (0.85 gr.) steel spheres penetrating gelatin.

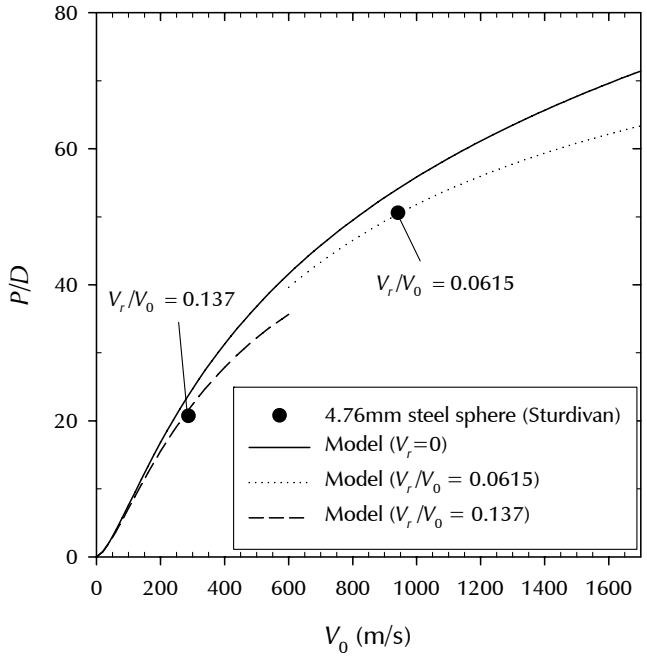

Figure 7. Normalized penetration *vs.* striking velocity for 4.76 mm (7 gr.) steel spheres penetrating gelatin.

The data for 16 gr. steel spheres from Sturdivan are examined in figure 8. The match of the model to data is generally excellent, with the lone exception being the highest velocity datum whose penetration is several diameters beyond the predicted amount; nonetheless, this amounts to an error of less than 7%.

Finally, we consider the data of Minisi, collected for 4.445 mm steel spheres impacting at speeds below 300 m/s. The data and two corresponding fits are displayed in figure 9. When using the fitting parameters employed for the Sturdivan data set, the prediction was on the high side of the data. In order to match this limited data set better, one of the fitted parameters, V_c, was set to a larger value of 105 m/s.

As to why there is this slight systematic disparity, one possibility is offered here for consideration. Hydrated ballistic gelatin is a material unlike most targets of ballistic interest in that several key phases of the preparation are performed, not in a manufacuting plant but by the end user. These key phases include hydrating the gelatin powder to the right concentration in water of the proper temperature, mixing the solution to maximize homogeneity while minimizing void content, and refrigerating the hydrated liquid gelatin to the proper temperature until the material sets. With all these key phases in the hands of the end user, it is perhaps not surprising that if two laboratories were to start with the same gelatin powder, they might produce batches of 20% ballistic gelatin with slight, yet systematic variations in mechanical properties. Given that the Sturdivan and Minisi data sets were generated over 25 years apart in two different facilities, the author finds such a disparity of minor concern. To help clarify the nature of this data disparity, it would have been beneficial if the Minisi data could have been extended out to higher velocities.

Figures 6–9 portray the maximum penetration achieved by a variety of different spheres impacting over a large range of striking velocities. The corresponding curves, given by equation 17, which accounts for the effect of local strain rate, appear to provide excellent fits to the data. However, a better measure of the quality of the fit may be obtained by examining the decelerations of individual tests and their corresponding predictions according to equation 16. Figures 10–13 provide those curves for all the test data examined in this report where, as before, each figure depicts the data for a different sphere diameter. Despite some scatter in the data, the model captures very well the transitions from high-velocity deceleration, to mid-velocity penetration efficiency, to low-velocity arrest.

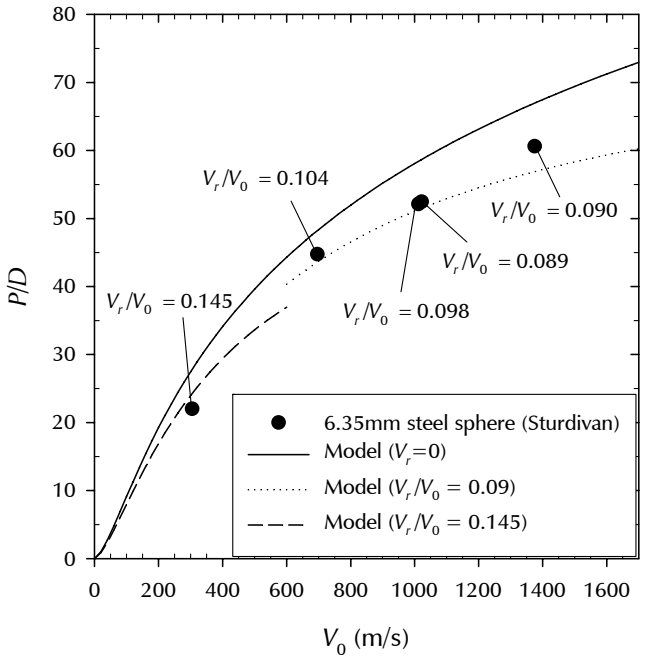

Figure 8. Normalized penetration *vs.* striking velocity for 6.35 mm (16 gr.) steel spheres penetrating gelatin.

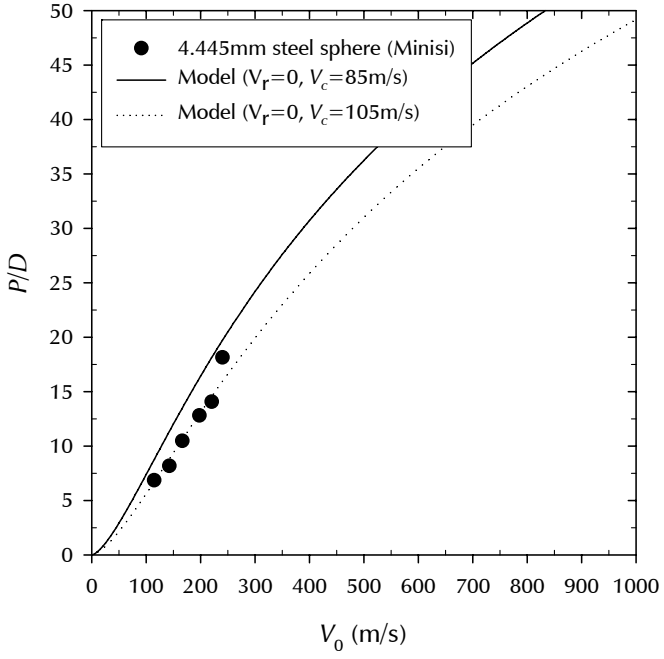

Figure 9. Normalized penetration *vs.* striking velocity for 4.445 mm steel spheres penetrating gelatin.

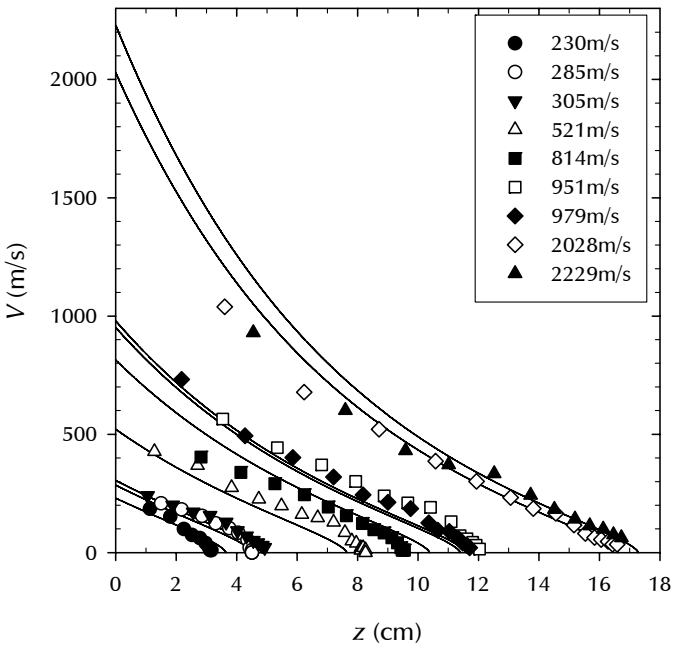

Figure 10. Velocity *vs.* position for 2.38 mm steel spheres of Sturdivan (*3*), with comparison to model predictions.

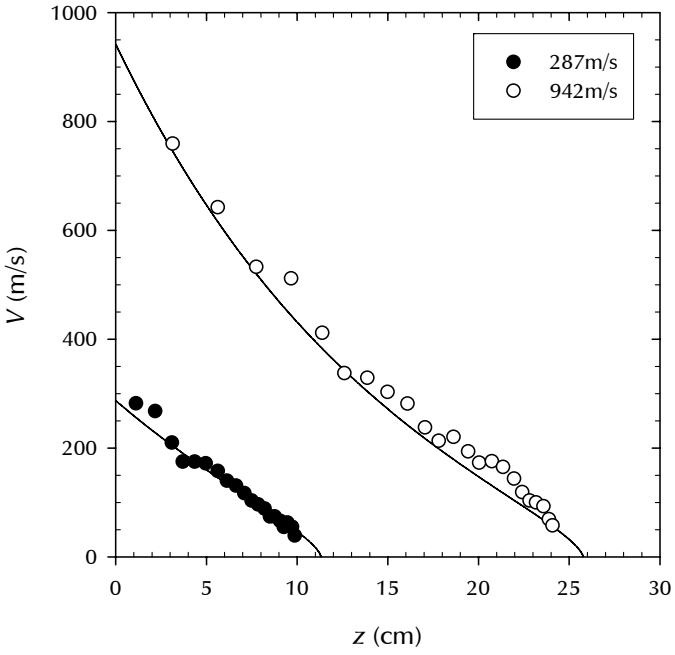

Figure 11. Velocity *vs.* position for 4.76 mm steel spheres of Sturdivan (*3*), with comparison to model predictions.

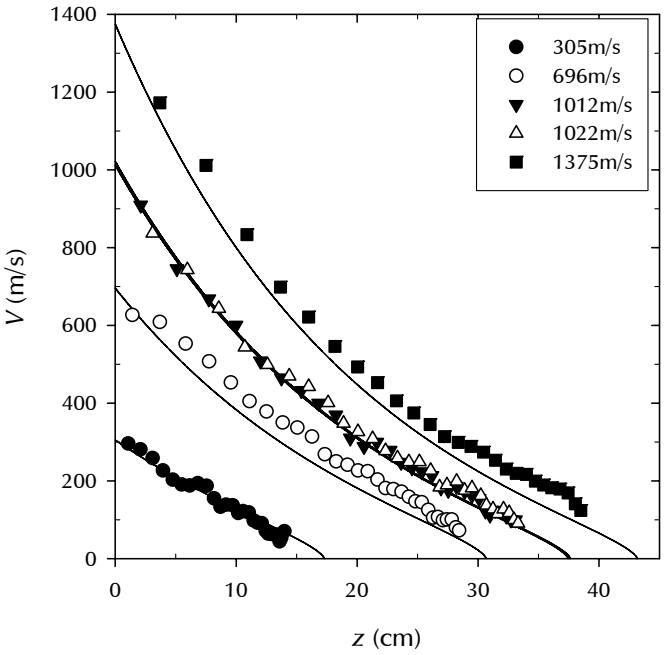

Figure 12. Velocity *vs.* position for 6.35 mm steel spheres of Sturdivan (*3*), with comparison to model predictions.

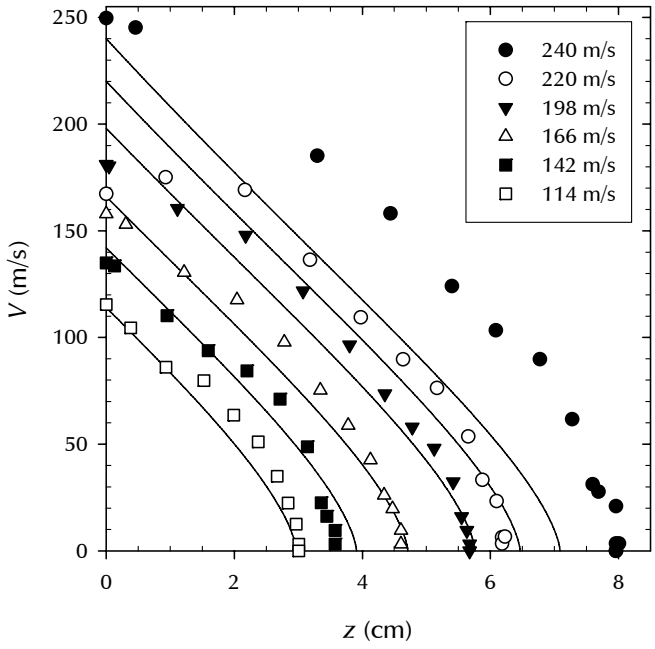

Figure 13. Velocity *vs.* position for 4.445 mm steel spheres of Minisi (*4*), with comparison to model predictions.

While Sturdivan did not publish V *vs.* x plots (only V *vs.* t), he did derive the equation characterizing the Resal's Law form that he utilized. The equation takes the form of

$$V = V_0 - c(1 - e^{-dx}) \quad . \tag{22}$$

Such a form does not change concavity…it is always concave upwards. The concave-downward "knee," which is invariably present at the lower right terminus of the curves in figures 10–13, cannot be modeled with Resal's Law, as Sturdivan himself admits. As such, a fit of Sturdivan's model to the high-velocity segment of the data will invariably lead to a systematic overestimation of the final penetration when Resal's Law is utilized. Likewise, an attempt to match the final penetration with Resal's Law will produce a poor fit of velocity over much of the deceleration. Such deficiencies do not apply to the currently proposed strain-rate dependent model.

Because of the fortuitous value of the fitted coefficient $\alpha = 1/2$, position *vs.* time is also implicitly available, by way of equations 20 and 16 (see figure 14 for an example).

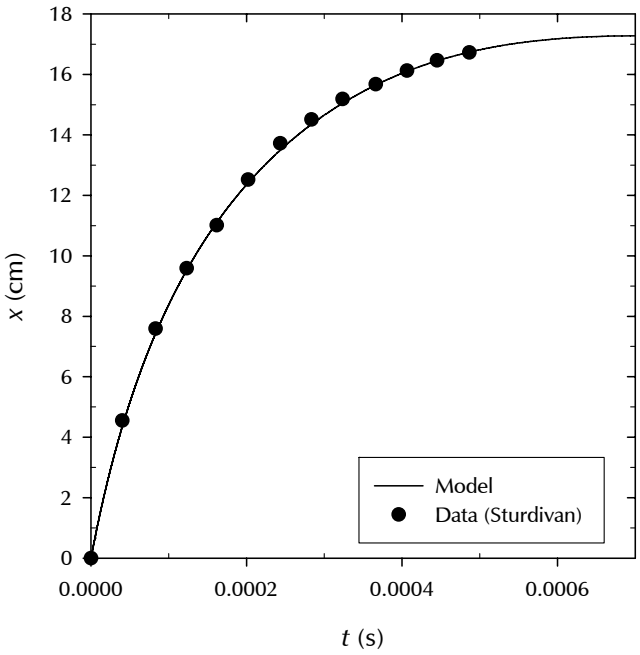

Figure 14. Position *vs.* time for 2.38 mm steel sphere of Sturdivan (*3*), impacting at 2229 m/s, with comparison to model predictions.

4. Conclusions

In this report, a model was proposed to characterize the resistance of gelatin to penetration by spherical penetrators. The proposed model differs from traditional resistance formulations, where the resistance is assumed to be a constant material property. It also differs from the gelatin model of Sturdivan (*3*), which treats the target resistance in terms of Newtonian viscosity. In the present model, the resistance is assumed to be a power of the strain rate, the actual exponent being a fitted parameter of the model. In this manner, the current model bridges the gap between a pure strength-based resistance formulation and a Newtonian-viscous formulation.

The net effect of a rate-dependent formulation for gelatin is that the target resistance varies with both penetration velocity as well as projectile diameter. The behavior of such a model was fitted to and compared against historical data of Sturdivan (*3*) as well as more recent data of Minisi (*4*). Over velocities which reached as high as 2229 m/s and over a range of sphere diameters from 2.38 mm to 6.35 mm, the model was shown to match the data in an excellent manner.

Unlike the Resal's Law formulation employed by Sturdivan, where the projectile velocity is always concave upward as a function of instantaneous penetration, the current model can and does capture the change in concavity in velocity *vs.* penetration, as the sphere is rapidly decelerated and brought to a halt in the latter stages of the event.

The general form of the current model is able to provide a closed-form solution for velocity *vs.* instantaneous penetration (*i.e.*, position). However, in the current case, because the fitted strain-rate exponent is exactly 1/2, there also exists a closed-form solution for time *vs.* velocity. In this manner, position *vs.* time results are available as an implicit function of velocity.

While comparison to data over a wider range of sphere diameters would be highly desirable to further validate the rate-dependence feature of the proposed model, the existing data nonetheless spans a respectable range of striking velocities and projectile diameters. Another problem worthy of future investigation would be to adapt the model for use with nonspherical projectiles. While such an adaptation should hopefully be straightforward for rigid, compact ($L/D \approx 1$) fragments, the modeling of eroding,

slender ($L/D > 1$), or flat ($L/D < 1$) projectiles would require additional considerations, especially if the penetration into gelatin were not aerodynamically stable.

5. References

1. Tate, A. A Theory for the Deceleration of Long Rods After Impact. *Journal of Mechanics and Physics of Solids* **1967,** *15,* 387–399.

2. Segletes, S. B.; Walters, W. P. Extensions to the Exact Solution of the Long-Rod Penetration/Erosion Equations. *International Journal of Impact Engineering* **2003,** *28,* 363–376.

3. Sturdivan, L. M. *A Mathematical Model of Penetration of Chunky Projectiles in a Gelatin Tissue Simulant*; ARCSL-TR-78055; U.S. Army Chemical Systems Laboratory: Aberdeen Proving Ground, MD, December 1978.

4. Minisi, M. *LS-Dyna Simulations of Ballistic Gelatin*; U.S. Army ARDEC: Picatinny Arsenal, NJ, report in progress, 31 October 2006.

5. Schlichting, H. *Boundary-Layer Theory;* 7th ed.; McGraw-Hill: New York, 1979 (first published in German as *Grenzschicht-Theorie*, 1951).

6. Beyer, W. H. *CRC Standard Math Tables;* 26th ed.; CRC Press: Boca Raton, 1981.

INTENTIONALLY LEFT BLANK.

NO. OF COPIES	ORGANIZATION
1 (PDF ONLY)	DEFENSE TECHNICAL INFORMATION CTR DTIC OCA 8725 JOHN J KINGMAN RD STE 0944 FORT BELVOIR VA 22060-6218
1	US ARMY RSRCH DEV & ENGRG CMD SYSTEMS OF SYSTEMS INTEGRATION AMSRD SS T 6000 6TH ST STE 100 FORT BELVOIR VA 22060-5608
1	DIRECTOR US ARMY RESEARCH LAB IMNE ALC IMS 2800 POWDER MILL RD ADELPHI MD 20783-1197
1	DIRECTOR US ARMY RESEARCH LAB AMSRD ARL CI OK TL 2800 POWDER MILL RD ADELPHI MD 20783-1197
1	DIRECTOR US ARMY RESEARCH LAB AMSRD ARL CI OK T 2800 POWDER MILL RD ADELPHI MD 20783-1197
	ABERDEEN PROVING GROUND
1	DIR USARL AMSRD ARL CI OK TP (BLDG 4600)

NO. OF COPIES	ORGANIZATION
1	COMMANDER ARMY ARDEC AMSTA CCH A M D NICOLICH PICATINNY ARSENAL NJ 07806-5000
1	COMMANDER US ARMY ARDEC AMSTA AR CCL B M MINISI PICATINNY ARSENAL NJ 07806-5000
3	COMMANDER US ARMY AMC AMSAM RD PS WF D LOVELACE M SCHEXNAYDER G SNYDER REDSTONE ARSENAL AL 35898-5247
1	COMMANDER US ARMY AVN & MIS RDEC AMSAM RD SS AA J BILLINGSLEY REDSTONE ARSENAL AL 35898
1	NAWC S A FINNEGAN BOX 1018 RIDGECREST CA 93556
3	COMMANDER NWC T T YEE CODE 3263 D THOMPSON CODE 3268 W J MCCARTER CODE 6214 CHINA LAKE CA 93555
4	COMMANDER NSWC DAHLGREN DIV D DICKINSON CODE G24 C R ELLINGTON W HOLT CODE G22 W J STROTHER 17320 DAHLGREN RD DAHLGREN VA 22448

NO. OF COPIES	ORGANIZATION
1	M G LEONE FBI FBI LAB EXPLOSIVES UNIT 935 PENNSYLVANIA AVE NW WASHINGTON DC 20535
7	LOS ALAMOS NATL LAB L HULL MS A133 J WALTER MS C305 C WINGATE MS D413 C RAGAN MS D449 E CHAPYAK MS F664 J BOLSTAD MS G787 P HOWE MS P915 PO BOX 1663 LOS ALAMOS NM 87545
19	SANDIA NATL LAB R O NELLUMS MS 0325 T TRUCANO MS 0370 M KIPP MS 0370 D B LONGCOPE MS 0372 A ROBINSON MS 0378 R LAFARGE MS 0674 B LEVIN MS 0706 M FURNISH MS 0821 D CRAWFORD MS 0836 E S HERTEL JR MS 0836 L N KMETYK MS 0847 R TACHAU MS 0834 L CHHABILDAS MS 1181 W REINHART MS 1181 T VOGLER MS 1181 D P KELLY MS 1185 C HALL MS 1209 J COREY MS 1217 C HILLS MS 1411 PO BOX 5800 ALBUQUERQUE NM 87185-0100
4	LLNL ROBERT E TIPTON L 095 DENNIS BAUM L 163 MICHAEL MURPHY L 099 TOM MCABEE L 095 PO BOX 808 LIVERMORE CA 94550

NO. OF COPIES ORGANIZATION

5 JOHN HOPKINS UNIV
APPLIED PHYSICS LAB
T R BETZER
A R EATON
R H KEITH
D K PACE
R L WEST
JOHNS HOPKINS RD
LAUREL MD 20723

4 SOUTHWEST RSRCH INST
C ANDERSON
S A MULLIN
J RIEGEL
J WALKER
PO DRAWER 28510
SAN ANTONIO TX 78228-0510

2 UC SAN DIEGO
DEPT APPL MECH & ENGRG
SVCS R011
S NEMAT NASSER
M MEYERS
LA JOLLA CA 92093-0411

1 UNIV OF ALABAMA BIRMINGHAM
HOEN 101
D LITTLEFIELD
1530 3RD AVE
BIRMINGHAM AL 35294-4440

3 UNIV OF DELAWARE
DEPT OF MECH ENGRG
J GILLESPIE
J VINSON
D WILKINS
NEWARK DE 19716

1 UNIV OF MISSOURI ROLLA
CA&E ENGNG
W P SCHONBERG
1870 MINOR CIR
ROLLA MO 65409

1 UNIV OF PENNSYLVANIA
DEPT OF PHYSICS & ASTRONOMY
P A HEINEY
209 S 33RD ST
PHILADELPHIA PA 19104

NO. OF COPIES ORGANIZATION

1 UNIV OF TEXAS AT AUSTIN
DEPT OF MECHANICAL ENGRG
E P FAHRENTHOLD
1 UNIVERSITY STATION C2200
AUSTIN TX 78712

1 UNIV OF UTAH
DEPT OF MECH ENGRG
R BRANNON
50 S CENTRAL CAMPUS DR
RM 2110
SALT LAKE CITY UT 84112-9208

1 VIRGINIA POLYTECHNIC INST
COLLEGE OF ENGRG
DEPT ENGRG SCI & MECH
R C BATRA
BLACKSBURG VA 24061-0219

2 AEROJET ORDNANCE
P WOLF
G PADGETT
1100 BULLOCH BLVD
SOCORRO NM 87801

2 APPLIED RSRCH ASSOC INC
D GRADY
F MAESTAS
STE A220
4300 SAN MATEO BLVD NE
ALBUQUERQUE NM 87110

1 APPLIED RSRCH LAB
T M KIEHNE
PO BOX 8029
AUSTIN TX 78713-8029

1 APPLIED RSRCH LAB
J A COOK
10000 BURNETT RD
AUSTIN TX 78758

1 BAE SYS ANALYTICAL
SOLUTIONS INC
M B RICHARDSON
308 VOYAGER WAY
HUNTSVILLE AL 35806

1 COMPUTATIONAL MECHANICS
CONSULTANTS
J A ZUKAS
PO BOX 11314
BALTIMORE MD 21239-0314

NO. OF COPIES ORGANIZATION

2 DE TECHNOLOGIES INC
R CICCARELLI
W FLIS
3620 HORIZON DR
KING OF PRUSSIA PA 19406

1 R J EICHELBERGER
409 W CATHERINE ST
BEL AIR MD 21014-3613

1 GB TECH LOCKHEED
J LAUGHMAN
2200 SPACE PARK STE 400
HOUSTON TX 77258

6 GDLS
W BURKE MZ436 21 24
G CAMPBELL MZ436 30 44
D DEBUSSCHER MZ436 20 29
J ERIDON MZ436 21 24
W HERMAN MZ435 01 24
S PENTESCU MZ436 21 24
38500 MOUND RD
STERLING HTS MI 48310-3200

3 GD OTS
D A MATUSKA
M GUNGER
J OSBORN
4565 COMMERCIAL DR #A
NICEVILLE FL 32578

4 INST FOR ADVANCED TECH
S J BLESS
J CAZAMIAS
J DAVIS
H FAIR
3925 W BRAKER LN STE 400
AUSTIN TX 78759-5316

1 INTERNATIONAL RSRCH ASSOC
D L ORPHAL
4450 BLACK AVE
PLEASANTON CA 94566

1 R JAMESON
624 ROWE DR
ABERDEEN MD 21001

NO. OF COPIES ORGANIZATION

1 KAMAN SCIENCES CORP
D L JONES
2560 HUNTINGTON AVE STE 200
ALEXANDRIA VA 22303

1 KERLEY TECHNICAL SERVICES
G I KERLEY
PO BOX 709
APPOMATTOX VA 24522-0709

2 NETWORK COMPUTING SERVICES INC
T HOLMQUIST
G JOHNSON
1200 WASHINGTON AVE S
MINNEAPOLIS MN 55415

ABERDEEN PROVING GROUND

61 DIR USARL
AMSRD ARL SL BB
R DIBELKA
E HUNT
J ROBERTSON
AMSRD ARL SL BD
R GROTE
L MOSS
J POLESNE
AMSRD ARL SL BM
D FARENWALD
G BRADLEY
M OMALLEY
D DIETRICH
AMSRD ARL WM BD
A ZIELINSKI
AMSRD ARL WM MC
E CHIN
L LASALVIA
AMSRD ARL WM MD
G GAZONAS
AMSRD ARL WM T
T W WRIGHT
AMSRD ARL WM TA
S SCHOENFELD
M BURKINS
N GNIAZDOWSKI
W A GOOCH
C HOPPEL
E HORWATH
D KLEPONIS
C KRAUTHAUSER
B LEAVY
M LOVE
J RUNYEON

NO. OF
COPIES ORGANIZATION

AMSRD ARL WM TB
R BITTING
J STARKENBERG
G RANDERS-PEHRSON
AMSRD ARL WM TC
R COATES
R ANDERSON
J BARB
N BRUCHEY
T EHLERS
T FARRAND
M FERMEN-COKER
E KENNEDY
K KIMSEY
L MAGNES
D SCHEFFLER
S SCHRAML
S SEGLETES
A SIEGFRIED
B SORENSEN
R SUMMERS
W WALTERS
C WILLIAMS
AMSRD ARL WM TD
T W BJERKE
S R BILYK
D CASEM
J CLAYTON
D DANDEKAR
M GREENFIELD
Y I HUANG
B LOVE
M RAFTENBERG
E RAPACKI
M SCHEIDLER
T WEERISOORIYA
H MEYER
AMSRD ARL WM TE
J POWELL

NO. OF
COPIES ORGANIZATION

2 AERONAUTICAL & MARITIME
RESEARCH LABORATORY
S CIMPOERU
D PAUL
PO BOX 4331
MELBOURNE VIC 3001
AUSTRALIA

1 DSTO AMRL
WEAPONS SYSTEMS DIVISION
N BURMAN (RLLWS)
SALISBURY
SOUTH AUSTRALIA 5108
AUSTRALIA

1 ROYAL MILITARY ACADEMY
G DYCKMANS
RENAISSANCELANN 30
1000 BRUSSELS
BELGIUM

1 DEFENCE RSRCH ESTAB SUFFIELD
D MACKAY
RALSTON ALBERTA TOJ 2NO
RALSTON
CANADA

1 DEFENCE RSRCH ESTAB SUFFIELD
J FOWLER
BOX 4000 MEDICINE HAT
ALBERTA TIA 8K6
CANADA

1 DEFENCE RSRCH ESTAB
VALCARTIER
ARMAMENTS DIVISION
R DELAGRAVE
2459 PIE X1 BLVD N
PO BOX 8800
CORCELETTE QUEBEC GOA 1R0
CANADA

4 ERNST MACH INSTITUT
V HOHL ER
E SCHMOLINSKE
E SCHNEIDER
K THOMA
ECKERSTRASSE 4
D-7800 FREIBURG I BR 791 4
GERMANY

NO. OF
COPIES ORGANIZATION

3 FRAUNHOFER INSTITUT FUER
KURZZEITDYNAMIK
ERNST MACH INSTITUT
H ROTHENHAEUSLER
H SENF
E STRASSBURGER
KLINGELBERG 1
D79588 EFRINGEN-KIRCHEN
GERMANY

3 FRENCH GERMAN RSRCH INST
G WEIHRAUCH
R HUNKLER
E WOLLMANN
POSTFACH 1260
WEIL AM RHEIN D-79574
GERMANY

1 NORDMETALL GMBH
L W MEYER
EIBENBERG
EINSIEDLER STR 18 H
D-09235 BURKHARDTSDORF
GERMANY

2 TU CHEMNITZ
L W MEYER (x2)
FAKULTAET FUER MASCHINENBAU
LEHRSTUHL WERKSTOFFE DES
MASCHINENBAUS
D-09107 CHEMNITZ
GERMANY

2 AWE
M GERMAN
W HARRISON
FOULNESS ESSEX SS3 9XE
UNITED KINGDOM

5 DERA
J CULLIS
J P CURTIS Q13
A HART Q13
K COWAN Q13
M FIRTH R31
FORT HALSTEAD
SEVENOAKS KENT TN14 7BP
UNITED KINGDOM